

LETTER TO THE EDITOR

The Broad Iron $K\alpha$ line of Cygnus X-1 as seen by *XMM-Newton* in the EPIC-pn Modified Timing Mode

Refiz Duro¹, Thomas Dauser¹, Jörn Wilms¹, Katja Pottschmidt^{2,3}, Michael A. Nowak⁴, Sonja Fritz^{1,5},
Eckhard Kendziorra⁵, Marcus G. F. Kirsch⁶, Christopher S. Reynolds⁷, and Rüdiger Staubert⁵

¹ Dr. Karl Remeis-Sternwarte and Erlangen Centre for Astroparticle Physics, Friedrich-Alexander-Universität Erlangen-Nürnberg, Sternwartstraße 7, 96049 Bamberg, Germany

² CRESST and NASA Goddard Space Flight Center, Astrophysics Science Division, Code 661, Greenbelt, MD 20771, USA

³ Center for Space Science and Technology, University of Maryland Baltimore County, 1000 Hilltop Circle, Baltimore, MD 21250, USA

⁴ Kavli Institute for Astrophysics, Massachusetts Institute of Technology, Cambridge, MA 02139, USA

⁵ Institut für Astronomie und Astrophysik, Eberhard Karls Universität Tübingen, Sand 1, 72074 Tübingen, Germany

⁶ European Space Agency, European Space Operations Centre, Robert-Bosch-Straße 5, 64293 Darmstadt, Germany

⁷ Department of Astronomy and Maryland Astronomy Center for Theory and Computation, University of Maryland, College Park, MD 20742, USA

Received XXX; accepted XXX

ABSTRACT

We present the analysis of the broadened, fluorescent iron $K\alpha$ line in simultaneous *XMM-Newton* and *RXTE* data from the black hole Cygnus X-1. The *XMM-Newton* data were taken in a modified version of the Timing Mode of the EPIC-pn camera. In this mode the lower energy threshold of the instrument is increased to 2.8 keV to avoid telemetry drop outs due to the brightness of the source, while at the same time preserving the signal to noise ratio in the Fe $K\alpha$ band. We find that the best-fit spectrum consists of the sum of an exponentially cut-off power-law and relativistically smeared, ionized reflection. The shape of the broadened Fe $K\alpha$ feature is due to strong Compton broadening combined with relativistic broadening. Assuming a standard, thin accretion disk, the black hole is close to maximally rotating.

Key words. X-rays: binaries – black hole physics – gravitation

1. Introduction

Relativistically broadened lines from accreting black holes have an important diagnostic potential as they allow us to measure directly properties of these black holes such as their spin, the inclination of the accretion disk, and the emissivity profile of the accretion disk (e.g., Reynolds & Nowak 2003). While by now a large number of high signal to noise ratio (S/N) measurements of the line shape and parameters exist for many Galactic black holes (Miller 2007) and for Active Galactic Nuclei (e.g., Miniutti et al. 2007; Fabian et al. 2009), high S/N measurements of the line profile and black hole parameters of the canonical black hole, Cygnus X-1, are still lacking. This lack is mainly due to a combination of source brightness, which causes the measurement to be dominated by systematic effects in the detector calibration (see, e.g., Miller et al. 2010), as well as a complex X-ray spectrum, which necessitates broad band (3–100 keV) measurements from multiple satellites. See, however, Miller et al. (2002) for recent work on the Fe line region with *Chandra*'s gratings, and Nowak et al. (2011, and references therein) on joint *Suzaku*/*RXTE* measurements of the broad band spectrum.

In this *Letter* we present an analysis of the broad band spectrum of Cygnus X-1 using data from high S/N observations of the Fe line band from *XMM-Newton* and simultaneous, 3–120 keV *RXTE* data. In Sect. 2 we present the Modified Timing Mode, a special flavor of the *XMM-Newton* Timing Mode, dedicated to bright sources with fluxes up to a few 100 mCrab. In

Sect. 3 we discuss the data reduction in greater detail. Section 4 presents the analysis of the relativistically broadened line and the reflection continuum.

2. The EPIC-pn Modified Timing Mode

To determine the best Fe line parameters possible, very high S/N observations are required in a time that is as short as possible to avoid complications due to source spectral variability. The best instrument currently fulfilling these requirements is the EPIC-pn camera onboard *XMM-Newton* (Strüder et al. 2001). This camera has two modes which provide the fast readout capability required to avoid pile up in bright source data (Ness et al. 2010). Here, the term “pile up” summarizes both “energy pile up”, where more than one X-ray photon impacts the same CCD pixel during one CCD readout cycle, and “pattern pile up” or “grade migration”, where multiple X-ray photons hit adjacent CCD pixels during one readout cycle and the resulting charge distribution in the CCD is wrongly interpreted as originating from a single, higher energy, X-ray. For satellites with moderate spatial resolution such as *XMM-Newton*, the latter effect is more pronounced. In EPIC-pn's Burst Mode, fast exposures and shifts are performed, interrupted by longer periods for data read out. The livetime of this mode is only 3%. In the Timing Mode, continuous read out is available with a 99.5% livetime. This mode is well suited for observations with a low pile up fraction for fluxes up to ~ 150 mCrab, although the EPIC-pn telemetry allo-

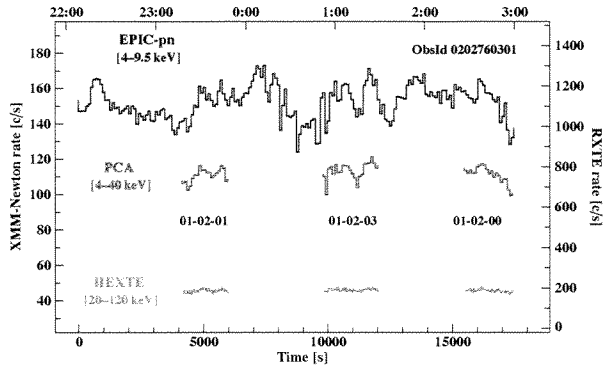


Fig. 1. *XMM-Newton* and *RXTE* lightcurve of Cygnus X-1 on 2004 November 20/21. Here, and throughout the remainder of the letter, EPIC-pn data are shown in blue, PCA (PCU2) data in red, and HEXTE in orange, with resolutions of 100 s, 96 s, and 40 s, respectively.

cation limits this mode to observations of sources of fluxes below ~ 100 mCrab. With ~ 300 mCrab, Cyg X-1 can therefore not be observed with the standard Timing Mode.

In order to address the telemetry limitation we have proposed a modification of the Timing Mode (Kendziorra et al. 2004). In this Modified Timing Mode, the lower energy threshold for telemetered events is increased from 0.15 keV to 2.8 keV, such that all events in the Fe line band can be transferred without telemetry drop outs, and the telemetry allocation to the EPIC-pn is maximized by switching off the EPIC-MOS cameras, which are piled up anyway for sources above ~ 35 mCrab.

EPIC data from events in which the charge cloud produced by an X-ray is distributed over more than one CCD pixel, so-called “split events”, are only recombined on ground. In the Modified Timing Mode, split partners with energies below 2.8 keV are not telemetered, resulting in a slight degradation of the energy resolution and necessitating the generation of a dedicated response matrix. As discussed by Wilms et al. (2006a) and Fritz (2008), this effect can be fully taken into account by measuring the energy dependent probability distribution of split events from archival Timing Mode observations and modifying the official Timing Mode response matrix accordingly. A full description of the calibration will be given in a forthcoming paper (Duro et al. 2011). The *XMM-Newton* data analysis and response matrix generation was based on the Science Analysis Software (SAS), version 10.0.0, and the newest calibration files.

It has recently been found that some Timing Mode observations are affected by “X-ray loading” (Done & Díaz Trigo 2009), i.e., the contamination of EPIC-pn’s offset map by source X-rays. Since the offset map is subtracted from the EPIC data before they are telemetered to ground, loading distorts the X-ray spectrum and effectively introduces a CCD-column dependent lower energy threshold. In the Modified Timing Mode, the offset map is determined with the EPIC-pn filter in the blocking position. As no source X-rays enter the offset map, the mode is unaffected by X-ray loading.

3. Data Reduction

3.1. Data Reduction

In 2004 fall *XMM-Newton* performed four Modified Timing Mode observations of Cyg X-1. Here, we concentrate on the simultaneous *XMM-Newton* and *RXTE* observations performed

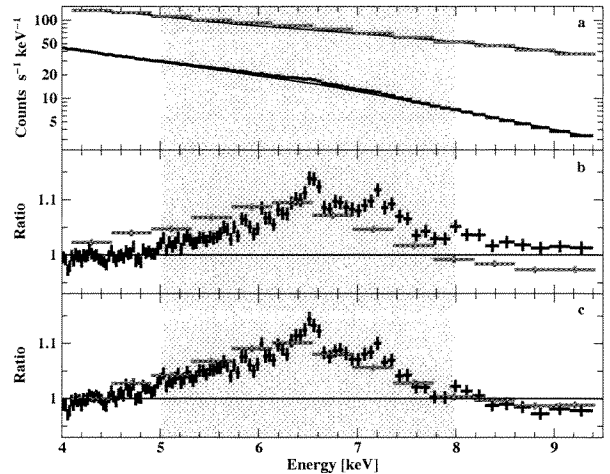


Fig. 2. **a** Fit of a simple power law to the 4.0–9.5 keV data, ignoring the 5.0–8.0 keV band (light gray area). **b** A broad excess due to the broad line, is visible. Note the energy shift between the PCA and the EPIC-pn. **c** Residuals after applying the gain shift correction.

2004 November 20 and 21 (*XMM-Newton* ID 0202760301), during which Cyg X-1 was in a transitional state between the hard state and the thermally dominated soft state (Fritz 2008). We concentrate on this 17.4 ks long observation since it shows the least variability on timescales of minutes to hours (Fig. 1) and thus provides the cleanest X-ray spectrum. Results from all observations will be presented in a subsequent paper (Duro et al. 2011). The increased soft X-ray emission during the intermediate state potentially leads to pile-up in the center of the point spread function. For the present study, we therefore ignore the innermost three columns. In order to avoid any transient effects due to the 2.8 keV lower energy threshold, we limit ourselves to the 4.0–9.5 keV band.

The simultaneous 6.18 ks of *RXTE* data (observation IDs 90104-01-02-00, -01, and -03) were reduced with HEASOFT version 6.9. We use the 4–40 keV data from the Proportional Counter Array (PCA; Jahoda et al. 2006) and the 20–112 keV data from the High Energy X-ray Timing Experiment (HEXTE; Rothschild et al. 1998) and ignore data taken within 10 minutes of passages through the South Atlantic Anomaly and during times of high particle background. All spectral analysis was done with the Interactive Spectral Interpretation System (Houck & Denicola 2000; Noble & Nowak 2008), HEXTE spectra were rebinned to $S/N = 30$, EPIC-pn to $S/N = 100$, resulting in a resolution of 40 eV at 6.4 keV and oversampling the detector response by a factor ~ 4 .

3.2. Simultaneous *XMM-Newton* and *RXTE* Fits

The 3–120 keV spectrum of Cyg X-1 can be well described as the sum of a soft excess with a temperature of $\lesssim 500$ eV, an exponentially cutoff power law with a cutoff at a few 100 keV, and a Compton reflection component (Nowak et al. 2011, and references therein). Alternatively, a variety of other, more physics based, components have been used to describe the continuum (Nowak et al. 2011; Malzac et al. 2008; Wilms et al. 2006b; Markoff et al. 2005), but these are virtually indistinguishable from this empirical model. In addition to the continuum components, *Chandra*-HETGS observations show the presence of a

narrow line at 6.4 keV emitted by neutral iron in material surrounding the black hole at larger distances (Hanke et al. 2009).

As shown in Fig. 2, a simple continuum model is not sufficient to describe the data. Strong positive residuals in the region between 5 and 7 keV remain, which are due to the broad Fe $K\alpha$ line. However, a slight mismatch in the *RXTE* and *XMM-Newton* residuals is also apparent (Figure 2b), with the EPIC line appearing to be shifted to a slightly higher energy. This shift is confirmed by measuring the energy of the 6.4 keV narrow line feature, which is found at 6.6 keV, inconsistent with all available *Chandra* measurements for this feature in Cyg X-1.

We attribute this difference to the treatment of charge transfer efficiency (CTE) effects in the SAS. When observing bright sources with a CCD such as the EPIC-pn, traps in the Silicon crystal can be saturated with source electrons, improving the CTE. While the latest SAS versions take this effect into account, their calibration breaks down for very high count rates. An overcorrection of CTE effects then leads to inferred photon energies that are too high. We take this effect into account by correcting the assigned photon energies with a model of the form $E_{\text{real}} = E_{\text{obs}}/s + \Delta E$. The model parameters s and ΔE are determined using measured energies of narrow spectral components or from continuum fitting. As will be discussed in greater detail by Duro et al. (2011), *Chandra*'s HETGS observation (obsid 3814) was taken at the same flux level as our *XMM-Newton/RXTE* observations. In addition to the 6.4 keV line, *Chandra* reveals two Fe $K\alpha$ absorption lines due to Fe xxv and Fe xxvi at 6.646 keV and 6.955 keV. Fits show that full consistency between the Modified Timing Mode spectrum and HETGS is obtained for $s = 1.02$ and $\Delta E = 0$ keV. This overcorrection of the EPIC energies by 2% is in line with typical CTE corrections for bright sources. An initial fit to the simultaneous 4–10 keV EPIC and PCA data agrees with this result (Fig. 2c), showing that the CTE correction can also be obtained from continuum fitting. The remaining differences between the EPIC and PCA data are due to narrow features which are not resolved by the PCA.

4. The Relativistic Broadened Fe $K\alpha$ Line of Cyg X-1

We now turn to modeling the broadened Fe line. To describe its profile we use the `re1line`-model of Dauser et al. (2010), a relativistic line model for thin disks around black holes with spins $-0.998 \leq a \leq +0.998$, where $a < 0$ indicates that the angular momenta of the black hole and the disk are antiparallel. We assume a radius-dependent line emissivity per disk unit area that scales $\propto r^{-\epsilon}$, where $\epsilon = 3$ for a thin accretion disk. The disk extends from the (a dependent) innermost stable circular orbit to $400GM/c^2$.

As expected, modeling the 4–10 keV spectrum with a simple relativistic line and a power-law continuum results in a bad fit ($\chi_{\text{red}}^2 \sim 1.5$) and unphysical line parameters as this approach does not take reflection self-consistently into account. We therefore extend the data to the full 4–120 keV band provided by EPIC-pn, PCA, and HEXTE, and model reflection of an exponentially cutoff power law self-consistently using the reflection model `relionx` (Ross & Fabian 2005). This model includes transitions from the most important ions, including Fe vi to Fe xxvi. In order to account for the relativistic smearing we convolve the reflected spectrum with a relativistic convolution model (`relconv`; Dauser et al. 2010). We assume that the angular distribution of the fluorescent photons is isotropic and due to photons emerging from a hot corona (Svoboda et al. 2009). In addition, we include narrow $K\alpha$ absorption lines from Fe xxv and Fe xxvi and a soft excess in the model.

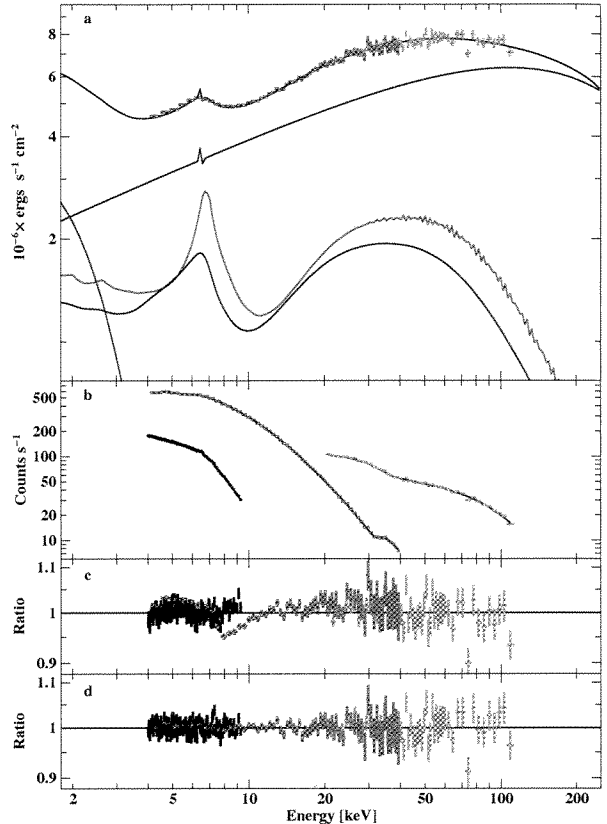


Fig. 3. **a** Unfolded *XMM-Newton* and *RXTE* data and best fit model components. Green line: reflection continuum in the frame of the disk (note the strong Compton broadening; the “jitter” above 50 keV is due to the numerical resolution of the reflection model). Purple line: relativistically smeared reflection component. **b** Measured count rate spectra. **c** Residuals of the best fit setting the relativistic convolution to zero. **d** Best fit residuals including relativistic convolution.

We first model the continuum using the canonical value of $\epsilon = 3$ for a thin accretion disk. As shown in Fig. 3 and Table 1, this model describes the 4–120 keV energy spectrum well, with a reduced $\chi_{\text{red}}^2 = 1.10$. The line profile indicates a high angular momentum of the black hole ($a = 0.88^{+0.08}_{-0.10}$, Fig. 4b), with further line broadening being due to strong Compton broadening in the strongly ionized reflector (ionization parameter $\xi = 1400^{+300}_{-100}$ erg cm s $^{-1}$), which smears out all other discrete features such as edges in the reflection spectrum (Fig. 3, green line). The inferred inclination is $32^\circ \pm 2^\circ$, in good agreement with most estimates for the inclination of the system (e.g., $32^\circ \leq i \leq 40^\circ$, Ninkov et al. 1987, $i < 55^\circ$, Sowers et al. 1998, or $36^\circ \leq i \leq 67^\circ$ Davis & Hartmann 1983). The Fe abundance is slightly higher than solar.

In order to check the uniqueness of this thin disk solution, a second fit letting ϵ free was performed. Figure 4 shows significance contours for this case. Most best-fit parameters are consistent between both fits, specifically, the inclination remains around 35° and the reflector remains strongly ionized. The emissivity, however, increases to $\epsilon = 10$ (the hard limit) while a decreases to 0. Broad lines can therefore be generated either by strongly concentrating all available emissivity to the innermost regions of a disk around a Schwarzschild black hole, or

Table 1. Best fit results to gainshifted EPIC-pn, PCA, and HEXTE data assuming an exponentially cutoff power law, a narrow emission line at 6.4 keV, two resonant absorption lines, disk black body emission, and relativistically convolved reflection. Fluxes and normalizations, A_i , are determined relative to the *RXTE*-PCA. C_{EPIC} and C_{HEXTE} are flux normalization constants for the EPIC and HEXTE, respectively. Uncertainties are at the 90% level for one interesting parameter.

Parameter	ϵ free	ϵ frozen
Γ_{pl}	$1.663^{+0.019}_{-0.017}$	1.670 ± 0.018
A_{pl}	$1.17^{+0.09}_{-0.08}$	$1.23^{+0.07}_{-0.08}$
E_{fold} [keV]	$290^{+0.08}_{-0.10}$	$290^{+0.08}_{-0.10}$
A_{bb}	$(0.44^{+0.19}_{-0.07}) \times 10^4$	$(0.54 \pm 0.07) \times 10^4$
$F_{6.4 \text{ keV}}$ [cgs]	$(0.6 \pm 0.2) \times 10^{-3}$	$(0.69^{+0.18}_{-0.20}) \times 10^{-3}$
$E_{\text{FeXXV } K\alpha}$ [keV]	6.646	6.646
τ_1	$(0.5 \pm 0.3) \times 10^{-2}$	$(0.4 \pm 0.3) \times 10^{-2}$
$E_{\text{FeXXVI } K\alpha}$ [keV]	6.955	6.955
τ_2	$\leq 2 \times 10^{-3}$	$\leq 1.9 \times 10^{-3}$
ξ [erg cm s $^{-1}$]	1700^{+300}_{-400}	1400^{+300}_{-200}
A_{reflionx}	$(1.2 \pm 0.3) \times 10^{-5}$	$(1.4 \pm 0.3) \times 10^{-5}$
Fe/Fe $_{\odot}$	$1.6^{+0.5}_{-0.4}$	$1.7^{+0.5}_{-0.4}$
a	-0.1 ± 0.4	$0.88^{+0.07}_{-0.11}$
i [deg]	36^{+2}_{-1}	32 ± 2
ϵ	10^{+0}_{-6}	3
C_{HEXTE}	0.830 ± 0.005	$0.830^{+0.006}_{-0.005}$
C_{EPIC}	0.785 ± 0.004	0.785 ± 0.004
$S_{\text{gainshift}}$	$1.0230^{+0.0019}_{-0.0017}$	$1.0240^{+0.0019}_{-0.0018}$
χ^2/dof	254/237	261/238
χ^2_{red}	1.08	1.10

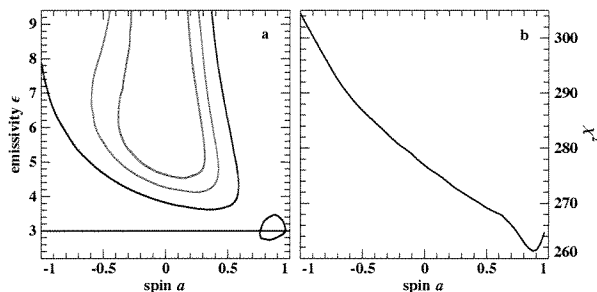


Fig. 4. **a** χ^2 significance contours for the emissivity index, ϵ , and the spin, a . Contours are based on $\Delta\chi^2 = 2.30, 4.61, \text{ and } 9.21$, i.e., 68%, 90%, and 99% confidence for two parameters of interest, with respect to the best fit case with ϵ let free. Two minima are apparent, one indicating a low spin black hole at an unphysically large ϵ , and one indicating an almost maximally spinning black hole consistent with emission from a thin accretion disk ($\epsilon = 3$). **b** χ^2 as a function of a for $\epsilon = 3$.

by emission from a standard disk around a maximally rotating black hole. Both solutions are comparable in statistical quality¹. Given that most physical scenarios for very steep emissivity profiles such as strongly torqued accretion disks (Agol & Krolik 2000) or strong illumination of the innermost disk due to strong light bending from a high latitude source (“lampost models”; Martocchia & Matt 1996) also require high a , the high spin solution is preferred on physical grounds. Cygnus X-1 is therefore plausibly close to maximally rotating.

To conclude, this first analysis of a data set taken in the EPIC-pn Modified Timing Mode confirms the capability of the

¹ For $\Delta\chi^2 = 7$ and 235, respectively 236 degrees of freedom, the F -test indicates no improvement by introducing a free disk emissivity at the 99% level.

EPIC-pn camera to observe sources up to several 100 mCrab, yielding high S/N measurements of the Fe line band. Coupled with broad band data from other satellites such as *RXTE*, *INTEGRAL*, or *Suzaku*, the Modified Timing Mode allows the high precision measurement of the physical parameters of black hole candidates, including their inclination, spin, and emissivity profile. Applying this analysis to Cyg X-1 shows that its black hole is likely a Kerr black hole if one assumes the accretion disk to be flat and illuminated from a Compton corona. This result is consistent with spin measurements from the accretion disk continuum (Gou et al. 2011). Being in a High Mass X-ray Binary, the black hole in Cyg X-1 is comparatively young. Our result indicates that it must have been born at close to maximum spin as expected in typical scenarios for black hole formation in supernovae (MacFadyen & Woosley 1999). In a next step, all four Modified Timing Mode observations will be considered (Duro et al. 2011).

Acknowledgements. This work was partly supported by the European Commission under contract ITN215212 “Black Hole Universe” and by the Bundesministerium für Wirtschaft und Technologie under Deutsches Zentrum für Luft- und Raumfahrt grants 50 OR 0701 and 50 OR 1001. This paper is based on observations obtained with *XMM-Newton*, an ESA science mission with instruments and contributions directly funded by ESA member states and NASA. We thank Norbert Schartel and the *XMM-Newton* operations team for agreeing to perform observations in a new and untested mode, Maria Díaz-Trigo for many useful discussions on CTE and pile up effects in the EPIC-pn camera, Manfred Hanke for his significant input concerning the data analysis and interpretation for black hole X-ray data, and Jérôme Rodriguez for his many insightful comments.

References

- Agol, E. & Krolik, J. H. 2000, *ApJ*, 528, 161
- Dauser, T., Wilms, J., Reynolds, C. S., & Brenneman, L. W. 2010, *MNRAS*, 409, 1534
- Davis, R. & Hartmann, L. 1983, *ApJ*, 270, 671
- Done, C. & Díaz Trigo, M. 2009, *MNRAS*, 407, 2287
- Duro, R., Dauser, T., Wilms, J., et al. 2011, *A&A*, in prep.
- Fabian, A. C., Zoghbi, A., Ross, R. R., et al. 2009, *Nature*, 459, 540
- Fritz, S. 2008, Dissertation, Eberhard-Karls Universität Tübingen
- Gou, L., McClintock, J. E., Reid, M. J., et al. 2011, *ApJ*, submitted (arXiv:1106.3690)
- Hanke, M., Wilms, J., Nowak, M. A., et al. 2009, *ApJ*, 690, 330
- Houck, J. C. & Denicola, L. A. 2000, in *ASP Conf. Ser. 216, Astronomical Data Analysis Software and Systems IX*, ed. N. Manset, C. Veillet, & D. Crabtree, 591–595
- Jahoda, K., Markwardt, C. B., Radeva, Y., et al. 2006, *ApJS*, 163, 401
- Kendziorra, E., Wilms, J., Haberl, F., et al. 2004, in *UV to Gamma-Ray Space Telescope Systems*, ed. G. Hasinger & M. J. L. Turner, Proc. SPIE 5488 (Bellingham, WA: SPIE), 613–622
- MacFadyen, A. I. & Woosley, S. E. 1999, *ApJ*, 524, 262
- Malzac, J., Lubiriski, P., Zdziarski, A. A., et al. 2008, *A&A*, 492, 527
- Markoff, S., Nowak, M. A., & Wilms, J. 2005, *ApJ*, 635, 1203
- Martocchia, A. & Matt, G. 1996, *MNRAS*, 282, L53
- Miller, J. 2007, *ARA&A*, 45, 441
- Miller, J. M., D’Ai, A., Bautz, M. W., et al. 2010, *ApJ*, 724, 1441
- Miller, J. M., Fabian, A. C., Wijnands, R., et al. 2002, *ApJ*, 578, 348
- Miniutti, G., Fabian, A. C., Anabuki, N., et al. 2007, *PASJ*, 59, 315
- Ness, J. U. et al. 2010, *XMM-Newton Users Handbook*, issue 2.8.1, ESA: ESAC, Villafranca
- Ninkov, Z., Walker, G. A. H., & Yang, S. 1987, *ApJ*, 321, 425
- Noble, M. S. & Nowak, M. A. 2008, *PASP*, 120, 821
- Nowak, M. A., Hanke, M., Trowbridge, S. N., et al. 2011, *ApJ*, 728, 13
- Reynolds, C. S. & Nowak, M. A. 2003, *Phys. Rep.*, 377, 389
- Ross, R. R. & Fabian, A. C. 2005, *MNRAS*, 358, 211
- Rothschild, R. E., Blanco, P. R., Gruber, D. E., et al. 1998, *ApJ*, 496, 538
- Sowers, J. W., Gies, D. R., Bagnuolo, W. G., et al. 1998, *ApJ*, 506, 424
- Strüder, L., Briel, U., Dennerl, K., et al. 2001, *A&A*, 365, L18
- Svoboda, J., Dovčiak, M., Goosmann, R., & Karas, V. 2009, *A&A*, 507, 1
- Wilms, J., Kendziorra, E., Nowak, M. A., et al. 2006a, in *Proc. X-ray Universe 2005*, ed. A. Wilson, ESA SP-604 (Noordwijk: ESA Publications Division), 217–222
- Wilms, J., Nowak, M. A., Pottschmidt, K., et al. 2006b, *A&A*, 447, 245